PASJ: Publ. Astron. Soc. Japan **58**, 965–977, 2006 December 25

A RIAF Interpretation for the Past Higher Activity of the Galactic Center Black Hole and the 511 keV Annihilation Emission

Tomonori TOTANI
Department of Astronomy, Kyoto University, Sakyo-ku, Kyoto 606-8502
totani@kusastro.kyoto-u.ac.jp

(Received 2006 July 19; accepted 2006 September 12)

Abstract

There are several lines of evidence to show that the supermassive black hole at the Galactic center had higher activities in the past than directly observed at present. It is shown here that these lines of evidence can quantitatively and consistently be explained if the mean accretion rate during the past $\sim 10^7$ yr has been $\sim 10^{3\text{–}4}$ times higher than the current rate, based on the picture of radiatively inefficient accretion flow (RIAF) and associated outflow that has been successfully applied to Sgr A*. We argue that this increased rate and its duration are theoretically reasonable in the Galactic center environment, while the accretion rate suddenly dropped about 300 yr ago, most likely because of the shell passage of the supernova remnant Sgr A East. The chance probability of witnessing Sgr A* in such a low state is not extremely small ($\sim 0.5\%$). The outflow energetics is sufficient to keep the hot (~ 8 keV) diffuse gas observed in the Galactic center region. It is then shown that a significant amount of positrons should have been created around the event horizon during the higher activity phase, and injected into interstellar medium by the outflow. The predicted positron production rate and propagation distance are close to those required to explain the observed 511 keV annihilation line emission from the Galactic bulge, giving a natural explanation for the large bulge-to-disk ratio of the emission. The expected injection energy into interstellar medium is $\sim$ MeV, which is also favorable for an explanation of the 511 keV line emission.

Key words: accretion, accretion disks — Galaxy: center — gamma rays: observations

1. Introduction

A variety of active and high-energy phenomena are seen in the direction toward the Galactic center over a broad range of wavelengths. It is well established that the center of our galaxy, Sagittarius (Sgr) A*, is a supermassive black hole (SMBH) with a mass of $M_\bullet \sim 3 \times 10^6\, M_\odot$ (Genzel et al. 1997; Schödel et al. 2003); a number of models have been proposed to explain the radiation and its spectral energy distribution (SED) from Sgr A* by accretion of matter onto it (see Baganoff et al. 2003 for a review and comparison to X-ray observations). The concept of radiatively inefficient accretion flow (RIAF) is theoretically well motivated based on the physics of accretion flows, and models based on the RIAF picture have successfully been applied to many low accretion rate systems with $\dot{M} \lesssim 0.1 \dot{M}_{\rm Edd}$, where $\dot{M}_{\rm Edd}$ is the Eddington mass accretion rate (Narayan, Quataert 2005 for a review). Sgr A* is one of the best-studied examples, and the model of Yuan, Quataert, and Narayan (2003, 2004, hereafter YQN03 and YQN04, respectively) can reproduce the observed SED of Sgr A* over a wide range of wavelengths from radio to X-ray bands. An important ingredient of this model is that the accretion rate decreases with decreasing radius from the SMBH, indicating a significant mass loss by a magnetically driven outflow or wind. This is necessary to make the model consistent with observations, and such wind activities are also supported by recent numerical simulations (YQN03 and references therein).

Though this model can explain the SED of Sgr A* at present, there are several lines of evidence for higher activities at the Galactic center in the past, such as much higher X-ray luminosity and mass outflows (see section 3 for a brief review). Hence, it is interesting to examine whether these lines of evidence can consistently be explained by changing the accretion rate within the framework of the RIAF model. The first aim of this paper is to show that it is indeed possible; it is also discussed whether such a high accretion rate is reasonable in the environment of the Galactic center, as well as the cause of the sudden decrease leading to the current low rate.

The 511 keV electron-positron annihilation line emission in the Galaxy has been observed for a long time (Knödlseder et al. 2005 and references therein), and the latest observation by the INTEGRAL gamma-ray observatory revealed that the all-sky distribution is dominated by the extended bulge component ($\sim 8^\circ$ FWHM), with weak evidence for the disk component (Knödlseder et al. 2005). Although the disk component can be explained by positron emission from radioactive nuclei produced in supernovae, the origin of the bulge component is still a mystery. A positron production rate of $\sim 1.5 \times 10^{43}\,{\rm s}^{-1}$ is required to explain the bulge component.

A number of candidates have been proposed for the origin of the bulge component, but the large bulge-to-disk ratio excludes many of them related to recent star-formation activities, leaving type Ia supernovae (SNe Ia) and low-mass X-ray binaries (LMXBs) as the primary candidates (Knödlseder et al. 2005 and references therein). However, about an order of

magnitude higher rate of bulge SNe Ia than the best estimate is required to explain the observed annihilation rate (Prantzos 2006). The positron production rate from LMXBs or microquasars is highly uncertain and might be sufficient (Guessoum et al. 2006), but the bulge-to-disk ratio of LMXBs is considerably lower than that of the 511 keV data. Most of the positrons produced in microquasars are probably lost by annihilation before injection into interstellar medium (ISM) (Guessoum et al. 2006), and direct annihilation gamma-ray emission from the sources would be inconsistent with the diffuse gamma-ray background around the MeV band (see subsection 6.3). The annihilation of dark-matter particles with a mass of $\sim$ MeV is another possible solution, but such a particle is not naturally predicted by particle physics theory, in contrast to well-motivated candidates, such as supersymmetric particles having much larger masses ($m_\chi \gtrsim 50$ GeV, Bertone et al. 2004). Furthermore, the upper limit on 511 keV line flux from the Sagittarius dwarf galaxy excludes this scenario for almost all types of the halo density profile (Knödlseder et al. 2005).

The second aim of this paper is to show that, if the past accretion rate onto Sgr A* was in fact higher than now with the rate and duration inferred from the observational evidence mentioned above, the RIAF model of Sgr A* gives a natural explanation for the bulge 511 keV line emission. There are models of positron production by accretion activity of Sgr A* (Titarchuk, Chardonnet 2006; Cheng et al. 2006), but the model proposed here is vastly different from these and it gives a more natural explanation for the 511 keV line (subsection 8.1).

A variety of phenomena on various scales around the Galactic center are discussed in this paper, and these are summarized in schematic diagrams in figure 1 for the reader's convenience. A summary of various comparisons between observations and the model is given in table 1. Starting from a brief description about the RIAF model of Sgr A* (section 2), the lines of evidence are reviewed and summarized for the past increased activity of Sgr A*, and RIAF interpretations are presented for these in section 3. The physical origin of the past high activity in the Galactic center environment is discussed in section 4. The positron production rate around the event horizon of Sgr A* is then calculated in section 5, and the ejection from Sgr A* (section 6) and propagation in ISM (section 7) are considered. In section 8, the present model is compared with the other models of the 511 keV emission, and future observational tests of this model are discussed. A distance of 8 kpc is applied to the Galactic center (Eisenhauer et al. 2003).

2. The RIAF Model of Sgr A* and Outflow

The YQN03 model is a one-dimensional, global RIAF model that can reproduce the SED of Sgr A*. Though the detailed three-dimensional structure is not taken into account in this model, models or simulations incorporating more complicated structures have not yet succeeded to reproduce the Sgr A* SED (e.g., Mineshige et al. 1995; Ohsuga et al. 2005). In this paper the scaling of the radiation and outflow from Sgr A* are discussed for the case when the accretion rate is changed, and the simple YQN03 model is sufficient and currently the best choice for this purpose.

The accretion rate of the YQN03 model is normalized at the outer boundary corresponding to the Bondi radius ($r_B \sim 10^5 r_s = 0.029$ pc), which is inferred from the ambient density and temperature of X-ray emitting gas (Baganoff et al. 2003), where r_s is the Schwarzschild radius of the SMBH. The size of the extended ($\sim 1''.4$ FWHM) X-ray emission of Sgr A* (Baganoff et al. 2003) nicely corresponds to this radius. The accretion rate at this radius is $\dot{M}_{acc}(r_B) \sim \alpha_v \dot{M}_B \sim 10^{-6}\, M_\odot\, \mathrm{yr}^{-1}$, where $\alpha_v \sim 0.1$ is a dimensionless viscosity parameter and $\dot{M}_B$ is the Bondi accretion rate. The YQN03 model assumes a radially varying accretion rate, $\dot{M}_{acc} \propto r^s$ with $s = 0.27$, based on adiabatic inflow-outflow solutions (ADIOS, Blandford, Begelman 1999), rather than advection dominated accretion flow (ADAF, see Kato et al. 1998; Narayan et al. 1998 for reviews), which is the simplest RIAF solution with a radially constant mass accretion rate. This modification from ADAF is necessary since the ADAF model predicts too-large density and magnetic field strength in the innermost region, in contradiction to the observational upper bounds on the rotation measure.

The accretion flow is quasi-spherical and the density, ρ, is determined by $\dot{M}_{acc}(r) \sim 4\pi\rho r^2 v_{in}$, where v_{in} is the inflow velocity of the accretion flow. In the self-similar solution of RIAFs, v_{in} is close to and proportional to the free-fall velocity, v_{ff}, and hence $\rho \propto r^{-3/2+s}$. In the YQN03 model, the particle density is $n_e \sim \rho/m_p \sim 3.9 \times 10^7 (r/r_s)^{-1.23}\, \mathrm{cm}^{-3}$, where m_p is the proton mass, and hence $v_{in} \sim 0.15\, v_{ff}$. This also means $\rho \propto \dot{M}_{acc}$.

It is reasonable to assume that the evaporated mass flow due to the nonconserving accretion rate is ejected as wind or outflow, whose velocity is comparable to the escape velocity, v_{esc}, at the region where the wind originates. Then, the mass-ejection rate per logarithmic interval of radius is $\dot{M}_w = r\,(d\dot{M}_{acc}/dr) = s\,\dot{M}_{acc}$, and the largest kinetic energy is produced from the innermost region where v_{esc} is close to the speed of light, c. We denote $r \sim r_*$ for the wind production region, and the outflow kinetic energy from this region becomes $L_{kin} \sim \dot{M}_w v_{esc}^2/2 \sim 1.5 \times 10^{38} r_3^{-0.73}\, \mathrm{erg\,s}^{-1}$, where $r_3 \equiv r_*/(3 r_s)$.

The jet or outflow may also contribute to the Sgr A* SED, especially in the radio bands (see discussion of YQN03). The outflow kinetic energy derived here is in fact comparable to those assumed in the jet models of Sgr A* (Falcke, Biermann 1999; Yuan et al. 2002; Le, Becker 2004), indicating that this estimate is a reasonable one.

The outflow kinetic power is much larger than the X-ray luminosity of Sgr A*, which is $L_X \sim 10^{33}\, \mathrm{erg\,s}^{-1}$ in the quiescent state and $\sim 10^{34\text{–}35}\, \mathrm{erg\,s}^{-1}$ in the flaring state. Such a trend of jet-energy dominance is indeed established for black holes in stellar X-ray binaries in the low/hard state (Gallo et al. 2003, 2005), which is believed to be a state corresponding to RIAF (Esin et al. 1997, hereafter EMN97). In fact, the above-mentioned kinetic and X-ray luminosities are consistent with the relation inferred for the stellar black hole binaries: $l_{kin} = f\,(l_X/0.02)^{0.5}$ with $f = 0.06$–1, where l_{kin} and l_X are in units of the Eddington luminosity (Gallo et al. 2005). Though the mass scale of black holes is quite different, this is expected if (1) the critical accretion rate in units of the Eddington rate ($\dot{M}/\dot{M}_{Edd}$) between the standard thin disk and RIAF is independent of the

black hole mass, (2) the X-ray luminosity scales roughly as $\dot{M}_{\rm acc}^2$ in the RIAF regime, and (3) the mass outflow is proportional to $\dot{M}_{\rm acc}$. The first two are indeed the properties of the ADAF (Narayan et al. 1998), and the third is in accordance with the radially varying accretion rate assumed in YQN03.

Some active galactic nuclei (AGNs) show jet activity with much higher speed (the bulk Lorentz factor $\Gamma \sim 10$) than the above velocity estimate ($\sim v_{\rm esc}$, only mildly relativistic with $\Gamma \sim 1$). However, $\Gamma \sim 1$ for Sgr A* is reasonable, since the same trend has been known for the outflows from stellar X-ray binaries in the low/hard state, which are not strongly beamed and not extremely relativistic ($\Gamma \lesssim 2$), in contrast to those of X-ray transients (Gallo et al. 2003; Narayan, McClintock 2005).

3. Past Higher Activity and RIAF Interpretation

3.1. Higher X-Ray Luminosity

There are a few independent lines of evidence that about 300 yr ago Sgr A* was much more luminous than now in the X-ray band. Koyama et al. (1996) found fluorescent X-ray emission reflected from cold iron atoms in the giant molecular cloud Sgr B2 by an ASCA observation (figure 1). Since there is no irradiation source to explain the iron line emission, they suggested a possibility that ~ 300 yr ago Sgr A* was much brighter than now. More recent studies by Murakami et al. (2000, 2001a, b) found a new X-ray reflection nebula associated with Sgr C, and estimated the increased past luminosity of Sgr A* as $L_{\rm X} \sim 3 \times 10^{39}\,{\rm erg\,s^{-1}}$ from Sgr B2 and C data. This claim was independently confirmed by an INTEGRAL observation covering a higher energy band of 10–100 keV (Revnivtsev et al. 2004); the ASCA and INTEGRAL data of Sgr B2 can be nicely fit by a reflection of radiation from Sgr A*, if its luminosity is $1.5 \times 10^{39}\,{\rm erg\,s^{-1}}$ in 2–200 keV and its spectrum is a power-law with a photon index of $\beta = 1.8 \pm 0.2$ ($dN/dE \propto E^{-\beta}$).

"The ionized halo" surrounding Sgr A* with a density $n_{\rm e,h} \sim 10^2$–$10^3\,{\rm cm^{-3}}$ has been known from radio observations (Pedlar et al. 1989; Anantharamaiah et al. 1999), and it extends to a radius of ~ 10 pc (figure 1). Maeda et al. (2002) argued that currently no ionizing source is found for the ionized halo, and the past activity of the Sgr A* may be responsible for the ionization, requiring an X-ray luminosity of $L_{\rm X} \sim 10^{40}\,{\rm erg\,s^{-1}}$, a similar flux to those inferred from the X-ray reflection nebulae.

We can then estimate the boost factor of the accretion rate to achieve the X-ray luminosity of $L_{\rm X} \sim 10^{39}$–$10^{40}\,{\rm erg\,s^{-1}}$ in the RIAF model. It should be noted that this luminosity is $\sim 10^{-5}$ in units of the Eddington luminosity, and hence it is still well within the ADAF/RIAF regime. According to figure 5 of YQN04, a boost factor of $f_{\rm b} \equiv \dot{M}_{\rm past}/\dot{M}_{\rm present} \sim 10^3$–$10^4$ (at a fixed radius r) is required to achieve a luminosity of $L_{\rm X} \sim 10^{39}$–$10^{40}\,{\rm erg\,s^{-1}}$, assuming a constant value for s. The SED in YQN04 with $f_{\rm b} \sim 10^3$ is roughly constant in νL_ν (luminosity per logarithmic frequency interval) in the X-ray band, being consistent with the X-ray spectrum inferred from the X-ray reflection nebula. Thus, the outflow kinetic luminosity in such a higher activity phase should be $L_{\rm kin} \sim 4.7 \times 10^{41} f_{3.5} r_3^{-0.73}\,{\rm erg\,s^{-1}}$, where $f_{3.5} \equiv f_{\rm b}/10^{3.5}$. In units of the Eddington mass accretion rate, $\dot{M}_{\rm Edd} = 10 L_{\rm Edd}/c^2$ (corresponding to a radiative efficiency of 0.1), the accretion rates at $r = r_{\rm B}$ and $r = r_{\rm s}$ are $4.6 \times 10^{-2} f_{3.5}$ and $2.1 \times 10^{-3} f_{3.5}$, respectively.

3.2. Mass Outflows on Various Scales

There is evidence for powerful mass outflow from the Galactic center on scales from arcminutes to tens of degrees (figure 1). Bland-Hawthorn and Cohen (2003) reported mid-infrared emission from dust expanding in the Galactic center lobe (GCL) on a few-degree scale, and estimated the total kinetic energy to be $\sim 10^{55}$ erg with a velocity of $\sim 100\,{\rm km\,s^{-1}}$ and a dynamical time of $\sim 10^6$ yr. The size, energy, and time scales are similar to those of the expanding molecular ring (EMR) around the Galactic center (Kaifu et al. 1972; Scoville 1972). Bland-Hawthorn and Cohen further argued that this result is consistent with the North Polar Spur (NPS) on an even larger scale (up to tens of degrees), which has been interpreted by Sofue (2000) to be an outflow from the Galactic center,[1] with an energy scale of $\sim 10^{55\text{–}56}$ erg and a dynamical time scale of $\sim 10^7$ yr. The kinetic luminosity inferred from these various observations is in good agreement with the estimate for the RIAF model with the boost factor of $f_{\rm b} \sim 10^{3\text{–}4}$, and hence we can attribute these outflows to the past activity of Sgr A*, which was responsible for the higher X-ray luminosity. This indicates a duration of $\sim 10^7$ yr for the higher activity, which is reasonable compared with various estimates for lifetimes of AGNs (Martini 2004).

The origin of the outflow from the Galactic center may instead be starbursts in the nuclear region, as suggested by Bland-Hawthorn and Cohen (2003). However, observations of gamma-rays from radioactive ^{26}Al seem to argue against the starburst scenario. An energy of 10^{55} erg in 10^6 yr is equivalent to ~ 1 supernova per century, almost comparable to the Galaxy-wide core-collapse supernova rate of 1.9 ± 1.1 per century (Diehl et al. 2006) estimated from the flux of ^{26}Al gamma-rays, whose spatial distribution is clearly associated along with the Galactic disk. Since the half-life of ^{26}Al is 7.2×10^5 yr, ^{26}Al cannot travel beyond the GCL region with an outflow velocity of $\sim 100\,{\rm km\,s^{-1}}$. Therefore, if the origin of the outflow is starburst, we can expect a strong ^{26}Al gamma-ray emission concentrated within a few degrees from the Galactic center, with a flux comparable to the total gamma-ray flux along with the disk. However, such a strong concentration at the Galactic center is not found (Prantzos, Diehl 1996; Knödlseder et al. 1999), indicating that the accretion activity of Sgr A* is more plausible as the origin of the mass outflow.

Muno et al. (2004) studied in detail the Chandra data of the diffuse X-ray emission within ~ 20 pc of the Galactic center; they concluded that the hard component plasma ($kT \sim 8$ keV, Koyama et al. 1989; Yamauchi et al. 1990) cannot be explained by unresolved point sources. The latest Suzaku observation by Koyama et al. (2006) further strengthened the case for a truly diffuse plasma (but see also Revnivtsev et al. 2006). If it is truly diffuse, it cannot be gravitationally bound, and requires a large

[1] There are other interpretations for NPS by closer objects on the Galactic disk, like a supernova remnant, but see Bland-Hawthorn and Cohen (2003) for arguments in favor of the Galactic center interpretation.

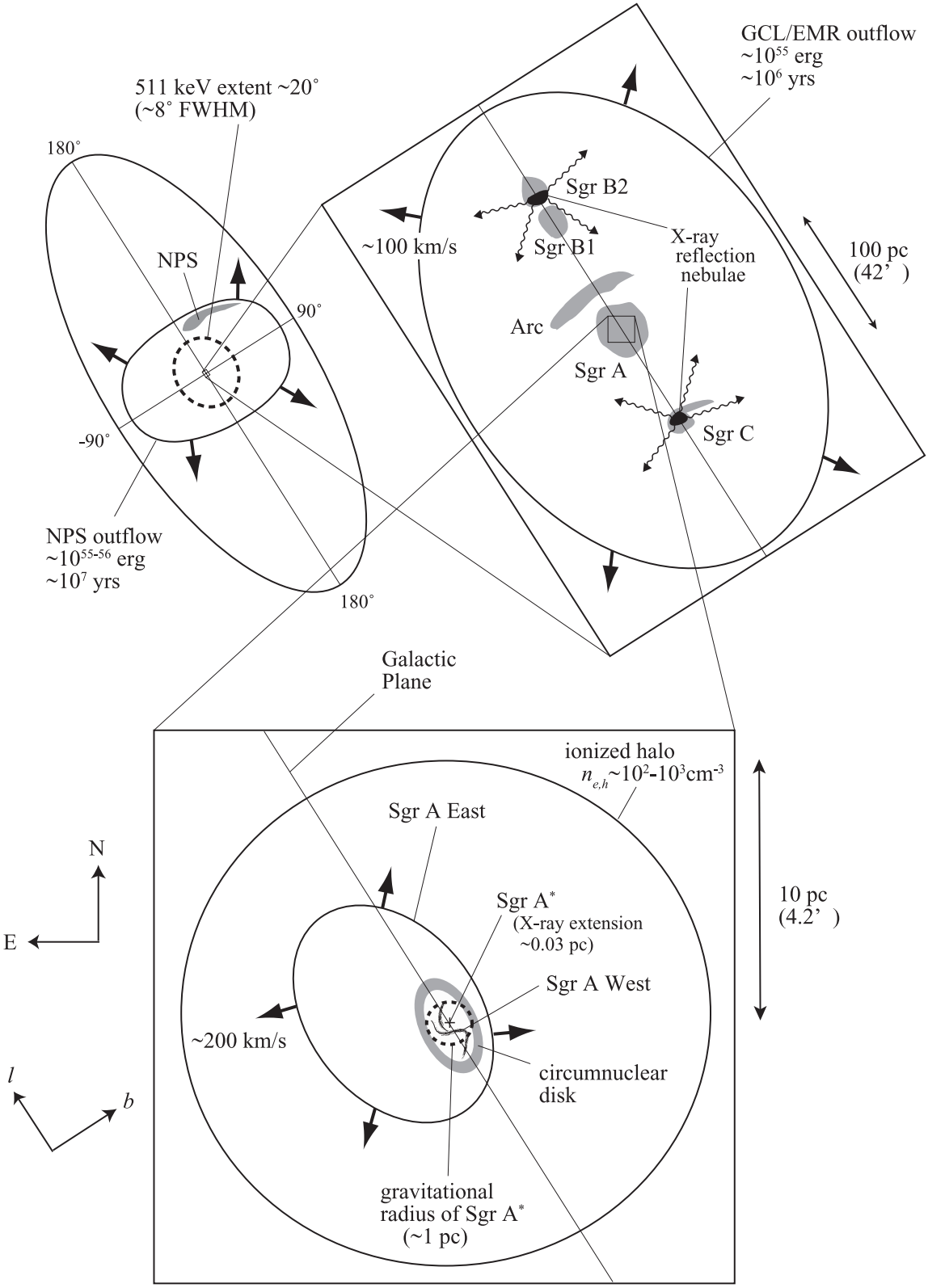

Fig. 1. Schematic diagrams for various phenomena on various scales around the Galactic center discussed in this paper. The upper-left diagram is the all sky map showing the scales of the 511 keV annihilation line emission and the outflow making the North Polar Spur (NPS). The upper-right diagram is for the region within $\sim 1^\circ$ of the Galactic center, showing the scale of the outflow observed as the Galactic center lobe (GCL) and the expanding molecular ring (EMR). Famous objects found in the radio image of this region are shown by grayscale, and the X-ray reflection nebulae are indicated by the black regions. The lower diagram is for the innermost region, showing the interaction of Sgr A East, West, and Sgr A* surrounded by the ionized halo. The gravitational radius (dashed circle) is a radius within which the SMBH gravity is dominant compared with the surrounding stars.

energy input of $\sim 10^{40}\,\mathrm{erg\,s^{-1}}$ to keep this hot plasma, when the escape time is estimated simply by the sound velocity. This is too large to be explained by supernova explosions, and the origin of this hot plasma is still a matter of debate. Later in this paper (subsection 7.1), the consequences of the energy injection into ISM by the wind from Sgr A* are discussed in more detail and it is shown that this hot plasma can be explained as a result of shock heating by the wind.

4. Origin of the Past Higher Activity

We have shown that all lines of evidence for the past higher activities of Sgr A* can be explained if the mean accretion rate in the past $\sim 10^7\,\mathrm{yr}$ is higher than now by a factor of $f_\mathrm{b} \sim 10^{3\text{–}4}$, and Sgr A* had such a high rate 300 yr ago. Then, the next questions are: (1) what is the source of the accreting matter during the high-activity phase, and (2) what caused the sudden drop of the accretion rate by a factor of $10^{3\text{–}4}$ on a time scale of just $\sim 10^{2\text{–}3}\,\mathrm{yr}$. Here, reasonable explanations for these questions are given.

4.1. The Role of Sgr A East and the Ionized Halo

Maeda et al. (2002) proposed that, based on their Chandra observation of the supernova remnant Sgr A East, the past higher activity was induced by accretion from the dense supernova shell expanding into the ionized halo. The location of Sgr A* is in fact inside Sgr A East and close to its shell (figure 1). In this scenario the duration of such a high accretion rate is only $\sim 10^3\,\mathrm{yr}$, as inferred from the shell thickness ($\sim 1/10$ of the observed shell radius $r_\mathrm{sh} = 2.9\,\mathrm{pc}$) and the shell expansion velocity ($v_\mathrm{sh} \sim 200\,\mathrm{km\,s^{-1}}$, estimated by a simple theoretical model of supernova remnants). For comparison, the age estimate of Sgr A East is $\sim 10^4\,\mathrm{yr}$. A much higher accretion rate than now is possible by Bondi accretion with the shell density estimated from shock-compression of the gas of the ionized halo. (The supernova ejecta are negligible at this stage.)

However, according to this scenario, we expect a comparable, or even higher, accretion rate by accretion directly from the ionized halo before passage of the Sgr A East shell, since the density enhancement by shock-compression is at most by a factor of 4, and the sound velocity of unshocked gas is likely to be much lower than the shell velocity. Suppose that the SMBH is embedded directly in the ionized halo. The Bondi radius in this case could be different from the current estimate (0.03 pc) based on the X-ray observation (Baganoff et al. 2003), since the current gas properties around Sgr A* have been altered from those of the ionized gas by passage of the Sgr A East shell. The Bondi radius in the halo, $r_\mathrm{B,h} = 2GM_\bullet/c_\mathrm{s,h}^2$ is larger than 1 pc if the temperature, kT_h, is lower than $\sim 110\,\mathrm{eV}$, where $c_\mathrm{s,h}$ is the sound velocity in the ionized halo. A plausible temperature of the ionized halo is $\sim 1\,\mathrm{eV}$ (Maeda et al. 2002), and hence the outer boundary of the accretion flow would not be determined by the Bondi radius, but rather by the gravitational radius, $r_\mathrm{grav} \sim 1\,\mathrm{pc}$, within which the gravity of the SMBH is dominant compared with stars around the SMBH (e.g., Schödel et al. 2003).

We can then extrapolate the YQN03 model from $r_\mathrm{B} = 0.029\,\mathrm{pc}$ out to r_grav with a boost factor of $f_\mathrm{b} \sim 10^{3\text{–}4}$ and $n_\mathrm{e} \propto r^{-1.23}$; the density at r_grav becomes $n_\mathrm{e} \sim 1.1 \times 10^3 f_{3.5}\,\mathrm{cm^{-3}}$. This is consistent with the density of the ionized halo, $n_\mathrm{e,h}$, and hence the RIAF at the increased accretion rate is naturally connected to the environment surrounding the SMBH. Since this is an extrapolation of the RIAF solution, the surrounding gas can accrete even if it has a significant angular momentum, because of the angular momentum loss by viscosity. This is in

Table 1. Summary of observations versus the model.

Observation	Scale (pc)	Requirement*	Prediction†	Section
Evidence for higher past X-ray luminosity				
X-ray reflection nebulae	100	$L_\mathrm{X} \sim 3 \times 10^{39}\,\mathrm{erg\,s^{-1}}$	$5 \times 10^{39} f_{3.5}$	3.1
Ionized halo	10	$L_\mathrm{X} \sim 10^{40}\,\mathrm{erg\,s^{-1}}$	$5 \times 10^{39} f_{3.5}$	3.1
Evidence for past outflow activity				
Galactic center lobe (GCL)	200	$L_\mathrm{kin} \sim 3 \times 10^{41}\,\mathrm{erg\,s^{-1}}$	$4.7 \times 10^{41} f_{3.5}$	3.2
Expanding molecular ring (EMR)	300	$L_\mathrm{kin} \sim 1 \times 10^{42}\,\mathrm{erg\,s^{-1}}$	$4.7 \times 10^{41} f_{3.5}$	3.2
North polar spur (NPS)	4×10^3	$L_\mathrm{kin} \sim 1 \times 10^{41}\,\mathrm{erg\,s^{-1}}$	$4.7 \times 10^{41} f_{3.5}$	3.2
8 keV diffuse gas	300	$E_\mathrm{hot} \sim 2.6 \times 10^{54}\,\mathrm{erg}$	$1.5 \times 10^{55} f_{3.5}$	3.2, 7.1
Evidence for pair production				
Bulge 511 keV line emission	600	$\dot{N}_+ \sim 1.5 \times 10^{43}\,\mathrm{s^{-1}}$		
		(production by ee)	$3.7 \times 10^{42} f_{3.5}^2$	5.4.1
		(production by $e\gamma$)	$8.1 \times 10^{41} f_{3.5}^3$	5.4.2
		(production by $\gamma\gamma$)	$1.1 \times 10^{42} f_{3.5}^4$	5.4.3

* X-ray luminosity (L_X), kinetic luminosity L_kin, energy stored in the hot gas (E_hot), or positron production rate ($\dot{N}_+$) required to explain the observations.

† The dependence on parameters other than the accretion rate is omitted, where $f_{3.5} = f_\mathrm{b}/10^{3.5}$ and $f_\mathrm{b} = \dot{M}_\mathrm{past}/\dot{M}_\mathrm{present}$.

contrast to the simple picture of spherical Bondi accretion.

In this new scenario, the high accretion rate can last for a much longer time scale than $\sim 10^3$ yr, and accretion from the dense supernova shell is no longer necessary. Still, Sgr A East must play an important role in explaining the sudden drop of the accretion rate ~ 300 yr ago, by the destruction of accretion flow when the dense shell passed through the SMBH. It should also be noted that there are the arm-like structures of Sgr A West and the circumnuclear disk surrounding it on a scale of ~ 1 pc (e.g., Yusef-Zadeh et al. 2000; see also figure 1), which could be remnants of the former accretion flow.

4.2. Destruction of the Accretion Flow by Sgr A East

We examine the destruction process more quantitatively as follows. Since the ADAF and ADIOS solutions have a positive Bernoulli parameter (Narayan et al. 1998; Blandford, Begelman 1999), the flow is not gravitationally bound, and a change of the flow velocity by an external force would result in destruction of the flow. Therefore, we should compare the momentum of the flow with that of the supernova remnant to estimate the effect of the supernova shell passage. The momentum of the accretion flow is

$$P_{\rm acc} \sim \frac{4\pi}{3} r^3 \rho\, v_{\rm flow} \tag{1}$$

$$\sim 5.6\times 10^{41}\left(\frac{r}{1\,{\rm pc}}\right)^{1.27} f_{3.5}\ \ {\rm g\,cm\,s^{-1}}, \tag{2}$$

where we estimated the flow velocity, $v_{\rm flow}$, by $\sim v_{\rm in}$, since the rotation velocity is negligible when the adiabatic index is $\gamma_{\rm ad} \to 5/3$ in ADAFs (Narayan et al. 1998). The momentum of the supernova remnant given to the flow is

$$P_{\rm SN} = \frac{1}{4}\left(\frac{r}{r_{\rm sh}}\right)^2 \frac{2E_{\rm SN}}{v_{\rm sh}} \tag{3}$$

$$\sim 3.0\times 10^{42}\left(\frac{r}{1\,{\rm pc}}\right)^2 \left(\frac{E_{\rm SN}}{10^{51}\,{\rm erg}}\right)\ \ {\rm g\,cm\,s^{-1}}, \tag{4}$$

where $E_{\rm SN}$ is the shell kinetic energy of the supernova remnant. Therefore, the accretion flow could have been destroyed at $r \gtrsim 0.1$ pc from the SMBH. Destruction should have occurred on a time scale of the shell crossing ($\sim 10^3$ yr), and the accretion time scale at this radius is also $r/v_{\rm in} \sim 1.3\times 10^3$ yr. These time scales are consistent with the required time scale of the accretion rate drop, ~ 300 yr. The current low rate may be determined by either the diffuse gas in the supernova remnant, winds from nearby stars (e.g., Cuadra et al. 2006), or residuals of the former accretion flow.

4.3. Comparison with Nearby Galaxies

We may ask how the suggested high activity of Sgr A* in the past compares with those found in nearby normal galaxies, because it would be statistically unlikely if our galaxy had a much higher activity in comparison with nearby normal galaxies. As reviewed by Ho (2004), nuclear activity is quite commonly found in nearby galaxies. The YQN04 model with $f_{\rm b} \gtrsim 10^3$ predicts a nuclear B-band luminosity of $L_B \sim 10^{39}\,{\rm erg\,s^{-1}}$; the number density of such galaxies expected from the nuclear luminosity function is $\sim 10^{-2}(h/0.75)^3\,{\rm Mpc^{-3}}$, which is similar to that of typical galaxies like our own, where $h = H_0/(100\,{\rm km\,s^{-1}\,Mpc^{-1}})$ is the Hubble constant. Nuclear radio cores with flux of 10^{19}–$10^{21}\,{\rm W\,Hz^{-1}}$ at 5 GHz are also commonly found, which is again a similar radio luminosity to that predicted by the YQN04 model with $f_{\rm b} \sim 10^{3\text{–}4}$. Therefore, the increased activity of Sgr A* is not particularly rare compared with nearby normal galaxies, indicating that the characteristic time scale of the increased activity can be $\sim 10^7$ yr, or even longer, possibly as long as the cosmological time scale. The accretion rate at the event horizon, i.e., the mass growth rate of the SMBH, is $1.4\times 10^{-4} f_{3.5}\, M_\odot\,{\rm yr^{-1}}$, and the mass growth in 10 Gyr is $1.4\times 10^6 f_{3.5}\, M_\odot$, which is still less than $M_\bullet$.

AGN activity is generally sporadic, and shows strong variability; hence, it is naturally expected that the accretion rate was always changing significantly in the past $\sim 10^7$ yr. In fact, the characteristic structures, such as GCL, EMR, and NPS, indicate such variability or modulation of the accretion and wind activity. However, the conclusions of this paper are not seriously affected if the mean or characteristic accretion rate is given by $f_{\rm b} \sim 10^{3\text{–}4}$.

4.4. Are We Living at a Very Special Time?

One may feel uneasy if we are witnessing a large drop in the accretion rate just during ~ 300 yr compared with the normal accretion time scale of $\sim 10^7$ yr, indicating an extremely low chance probability of observing Sgr A* in the present phase: $300/10^7 = 3\times 10^{-5}$. Here, it is argued that the actual chance probability is likely to be much larger than this simple estimate.

About 100 young massive stars are known to exist within the central parsec of Sgr A* (Paumard et al. 2006). Some of them are already in the post-main-sequence phase, and the age of this stellar population is estimated to be ~ 6 Myr. This indicates a supernova rate of $\sim 1.7\times 10^{-5}\,{\rm yr^{-1}}$, and the chance probability of observing Sgr A* within 300 yr after the shell passage becomes 0.5%. This is small, but not extraordinarily small for realization. The mean accretion rate can be kept at the level of $f_{\rm b} \sim 10^{3\text{–}4}$ if the accretion rate comes back to the mean level within the typical time interval of supernovae, $\sim 6\times 10^4$ yr, after shell passage.

It is an observational *fact* that we are living at a somewhat special time, if the association of Sgr A* with the Sgr A East shell is not just a superposition in the sky, but physical. The age of $\sim 10^4$ yr of Sgr A East indicates that the supernova rate within the central parsec of Sgr A* should be less than $10^{-4}\,{\rm yr^{-1}}$. Therefore, the chance probability must be less than $300/10^4 = 3\%$, which is just 6-times larger than the above estimate. Therefore, we consider that the argument of the chance probability does not seriously weaken the case for the overall picture proposed by this work.

5. Positron Production around Sgr A*

5.1. Physical Quantities around the Event Horizon

We now consider pair-production in the region where the wind originates, $r \sim r_*$. During the increased phase, the particle accretion rate is $\dot{N}_{\rm acc} = \dot{M}_{\rm acc}/m_{\rm p} \sim 7.1\times 10^{45} f_{3.5}\, r_3^{0.27}\ {\rm s^{-1}}$ and the particle outflow rate per logarithmic radius is $\dot{N}_{\rm w} = s\,\dot{N}_{\rm acc}$. The particle density in the accretion flow is

$n_e \sim 3.2 \times 10^{10} f_{3.5} r_3^{-1.23}\,\mathrm{cm}^{-3}$. The accretion time spent around this radius is $t_{acc} \sim r_*/v_{in} \sim 1.0 \times 10^3 r_3^{3/2}$ s.

The electron temperature of the YQN03 model is $T_e \sim 8 \times 10^{10} r_3^{-1}$ K, and hence the relative motion of the electrons is sufficiently relativistic in the pair-production region if $r_* \sim 3r_s$, with the mean electron Lorentz factor being $\gamma_e \sim 3.151 kT_e/(m_e c^2) \sim 40 r_3^{-1}$ in the rest frame of the accretion flow. The temperature does not heavily depend on the enhancement factor, $f_b \sim 10^{3.5}$, if the transfer efficiency of the viscous heating energy from ions to electrons (the parameter δ in YQN03) does not change with the accretion rate, as assumed in YQN04. It may increase with increasing accretion rate because of a higher density, and hence more efficient interactions, but the value of δ assumed in YQN03 is already of order unity (= 0.55), not leaving much room for an increase of δ.

5.2. Pair Equilibrium Criterion

The positron density produced in the accretion flow depends on whether the $e^\pm$ pair-production process achieves equilibrium with $e^\pm$ pair annihilation. This can be evaluated by comparing the pair-production rate density, $\dot{n}_+$, with the pair-annihilation rate density, $\dot{n}_{\pm,\mathrm{ann}} \equiv n_e n_+ \sigma_{\pm,\mathrm{ann}} c$, where n_+ is the produced positron density. The $e^\pm$ pair annihilation cross section is

$$\sigma_{\pm,\mathrm{ann}} = \frac{\pi r_e^2}{\gamma_\pm}[\ln 2\gamma_\pm - 1] \tag{5}$$

in the ultra-relativistic limit (Svensson 1982), where r_e is the classical electron radius and $\gamma_\pm$ is the Lorentz factor in the rest frame of one particle. Hence, $\gamma_\pm$ can be related as $\gamma_\pm \sim \gamma_+ \gamma_e$, where γ_+ is the positron Lorentz factor in the flow frame. Initially, the positron density is small, and it increases with time as $n_+ \sim \dot{n}_+ t$ until $t \sim t_{\pm,\mathrm{ann}}$ when the equilibrium is achieved ($\dot{n}_+ = \dot{n}_{\pm,\mathrm{ann}}$), where the pair annihilation time scale is $t_{\pm,\mathrm{ann}} \equiv (n_e c \sigma_{\pm,\mathrm{ann}})^{-1}$. Since $t_{\pm,\mathrm{ann}}$ does not depend on $\dot{n}_+$, the equilibrium condition is the same for any pair-production processes, and it is determined by comparing $t_{\pm,\mathrm{ann}}$ with the accretion time scale, as

$$\frac{t_{acc}}{t_{\pm,\mathrm{ann}}} = 4.2 \times 10^{-2} \gamma_+^{-1} f_{3.5} r_3^{1.27}, \tag{6}$$

where we have estimated the logarithmic part of the cross section with $\gamma_+ \sim \gamma_e \sim 40$.

For positrons produced by electron-electron scattering ($e^-e^- \to e^-e^-e^-e^+$), we expect $\gamma_+ \sim \gamma_e$, while for positrons produced by two-photon annihilation ($\gamma\gamma \to e^-e^+$) a variety of γ_+ is possible (see the following subsections). The positron energy may also significantly change by interactions with the accreting material within the accretion time scale. However, for any value of γ_+, we find that $t_{acc} \ll t_{\pm,\mathrm{ann}}$, and hence equilibrium will not be achieved, which means that we can estimate the pair density by $n_+ \sim \dot{n}_+ t_{acc}$.

5.3. Spectral Energy Distribution of Sgr A*

For pair-production processes including photons, we must assume the form of the SED and the emission region of Sgr A* during the increased activity phase. Here, we assume that the radiation is mainly coming from the region around the event horizon. It should be noted that the X-ray emission in the quiescent phase of the YQN03 model for present-day Sgr A* is dominated by thermal bremsstrahlung at large radii far from the SMBH, which is in agreement with the extended X-ray emission ($\sim 1''$). However, the synchrotron-self-Compton (SSC) component becomes dominant when the accretion rate is increased as $f_b \gtrsim 10^3$ (YQN04), and it is produced in the innermost region. Therefore, the above assumption for the higher activity phase is reasonable.

For the calculations presented below, a constant SED in νL_ν is assumed. The predicted SED of the YQN04 model when $f_b \gtrsim 10^3$ is approximately flat in νL_ν in the keV-to-MeV band. A flat νL_ν SED is also supported in the 2–200 keV band by the observed spectrum of the X-ray reflection nebula (subsection 3.1). Therefore, this assumption is well supported by both observation and theory in the photon energy band of keV–MeV.

The SED beyond MeV is more uncertain, and here we simply examine the constraints on the current SED of Sgr A*. The TeV gamma-ray emission detected by HESS from the inner 10′ of Sgr A* (Aharonian et al. 2004) is possibly coming from the region close to the event horizon, and its flux is similar to that extrapolated from X-ray bands with a constant νL_ν spectrum. Though the GeV flux of 3EG J1746−2851, which is the closest to Sgr A* among the EGRET sources, is considerably higher than the X-ray flux of Sgr A*, the poor angular resolution in this band does not allow one to establish a firm connection between the GeV flux and Sgr A* (Mayer-Hasselwander et al. 1998; Aharonian, Neronov 2005)[2]. Therefore, it is not unreasonable to assume a flat νL_ν SED at a photon energy of $\gtrsim$ MeV, though the uncertainty is large. On the other hand, the photon production region will become optically thick to $e^\pm$ pair production for very high-energy photons ($\gtrsim$ GeV), and the constant νL_ν assumption will be no longer valid at such a high-energy band (see subsubsection 5.4.3).

5.4. Expected Pair Amount in the Wind

We now estimate the expected amount of pairs produced by three processes of pair production, i.e., electron-electron scattering ($e^-e^- \to e^-e^-e^-e^+$), photon-electron collisions ($\gamma e^- \to e^-e^-e^+$), and two photon annihilation ($\gamma\gamma \to e^\pm$). The rates of the corresponding proton processes (e.g., $p\,e^- \to p\,e^-e^-e^+$) are about one order of magnitude smaller than these (Zdziarski 1982, 1985).

5.4.1. Electron-electron scattering

We used the formula given in Svensson (1982) for the cross section in the ultra-relativistic limit, which is $\sigma_{ee} = 1.7 \times 10^{-28}\,\mathrm{cm}^2$ for $\gamma_e = 40$, and depends on γ_e only logarithmically. Hence, the dependence on γ_e is ignored. Thus, the density ratio of the produced positrons to electrons is given as

$$\frac{n_+}{n_e} = \frac{\dot{n}_+ t_{acc}}{n_e} = c\,\sigma_{ee}\, n_e\, t_{acc} \tag{7}$$

$$= 1.6 \times 10^{-4} f_{3.5} r_3^{0.27}, \tag{8}$$

[2] A recent analysis of the EGRET data by Hooper and Dingus (2004) excluded Sgr A* as the origin of 3EG J1746−2851 beyond the 99.9% confidence level.

and hence the total positron production rate as an outflow from Sgr A* is

$$\dot{N}_+ \sim \dot{N}_{\rm w}\left(\frac{n_+}{n_{\rm e}}\right) \tag{9}$$

$$= 3.2\times10^{41} f_{3.5}^2 r_3^{0.54}\ \ {\rm s}^{-1}. \tag{10}$$

This is the rate per $\ln r_*$; integrating from $r_* = 3r_{\rm s}$ to $40\times3r_{\rm s}$, beyond which electrons become non-relativistic and hence the above formulations are no longer valid, the rate is increased by a factor of 11.7, leading to $\dot{N}_+ \sim 3.7\times10^{42} f_{3.5}^2\,{\rm s}^{-1}$. This estimate is, within the model uncertainties, in good agreement with the rate required for the bulge 511 keV emission, $1.5\times10^{43}\,{\rm s}^{-1}$ (Knödlseder et al. 2005).

5.4.2. Photon-electron collisions

The cross section for $e^-\gamma\rightarrow e^-e^-e^+$ depends on the photon frequency, $\nu_{\rm er}$, measured in the electron's rest frame, which is given by (Svensson 1982)[3]:

$$\sigma_{{\rm e}\gamma} = \frac{\pi\sqrt{3}}{972}\alpha\, r_{\rm e}^2 (x_{\rm er}-4)^2 \tag{11}$$

in the non-relativistic limit ($x_{\rm er}-4\ll4$), and

$$\sigma_{{\rm e}\gamma} = \alpha r_{\rm e}^2\left[\frac{28}{9}\ln(2x_{\rm er}) - \frac{218}{27}\right] \tag{12}$$

in the ultra-relativistic limit ($x_{\rm er}-4\gg4$), where $x_{\rm er}\equiv h\nu_{\rm er}/(m_{\rm e}c^2)$, α the fine-structure constant, and the reaction threshold $x_{\rm er,th}=4$.

Treating electrons as a single energy population with $\gamma_{\rm e}\sim40$, and estimating the photon number density per unit photon frequency (ν) in the laboratory frame as $n_\nu\sim L_\nu/(4\pi r_*^2 c\,h\nu)$, the positron production rate by this process can be written as

$$\dot{n}_+ = \int n_{\rm e} n_\nu \sigma_{{\rm e}\gamma}\, c\, d\nu \tag{13}$$

$$= \frac{\gamma_{\rm e} n_{\rm e}(\nu L_\nu)}{4\pi r^2 m_{\rm e}c^2}\int\frac{\sigma_{{\rm e}\gamma}(x_{\rm er})}{x_{\rm er}^2}dx_{\rm er}, \tag{14}$$

where we have used $\nu_{\rm er}\sim\gamma_{\rm e}\nu$. With the assumption of a flat νL_ν SED, the integration over $x_{\rm er}$ is mostly contributed from photons with $x_{\rm er}\sim20$, i.e., $h\nu\sim0.3\,{\rm MeV}$ for $\gamma_{\rm e}\sim40$. This target photon energy is within the range where the Sgr A* luminosity during increased activity can be reliably assumed, and hence the uncertainty about the luminosity and SED is small.

Then, the produced positron density is given by

$$\frac{n_+}{n_{\rm e}} = \frac{\dot{n}_+ t_{\rm acc}}{n_{\rm e}} \sim 4.2\times10^{-4} L_{39.5} r_3^{-1.5}, \tag{15}$$

where $L_{39.5} = \nu L_\nu/(10^{39.5}\,{\rm erg\,s^{-1}})$, and the total positron production rate in the outflow is

$$\dot{N}_+ \sim \dot{N}_{\rm w}\left(\frac{n_+}{n_{\rm e}}\right) \tag{16}$$

$$= 8.1\times10^{41} L_{39.5} f_{3.5} r_3^{-1.23}\ \ {\rm s}^{-1}. \tag{17}$$

Integration over $\ln r_*$ at $r_* > 3r_{\rm s}$ would slightly decrease the above number by a factor of 1/1.23. Though this number is smaller than the rate required to explain the 511 keV emission by about one order of magnitude, it may also be important if the model uncertainties are considered. Note that $L_\nu\propto\dot{M}_{\rm acc}^2$ at photon energies higher than the X-ray band in RIAFs, and hence $\dot{N}_+\propto f_{\rm b}^3$.

5.4.3. Photon-photon annihilation

Pair-production by two photon annihilation most efficiently occurs with a cross section of $\sigma_{\gamma\gamma}\sim1.7\times10^{-25}\,{\rm cm^{-2}}$, when the photon energy at the center-of-mass is about the electron mass, as $(h\nu_{\rm l}\,h\nu_{\rm h})^{1/2}\sim2m_{\rm e}c^2$, where $\nu_{\rm l}$ and $\nu_{\rm h}$ are the frequencies of two photons in the laboratory frame ($\nu_{\rm l}<\nu_{\rm h}$) (e.g., Salamon, Stecker 1998). For photons meeting this condition, the pair-production rate density is given by

$$\dot{n}_+ \sim \nu_{\rm h} n_\nu(\nu_{\rm h})\,\nu_{\rm l} n_\nu(\nu_{\rm l})\sigma_{\gamma\gamma}\, c, \tag{18}$$

which is constant against $\nu_{\rm h}$ (and $\nu_{\rm l}$) based on the assumption of constant νL_ν SED. It should be noted that this is valid only when the region is optically thin for high-frequency photons, i.e., $\tau_{\gamma\gamma}\lesssim1$, where

$$\tau_{\gamma\gamma} = \nu_{\rm l} n_\nu(\nu_{\rm l})\sigma_{\gamma\gamma}\, r_* \tag{19}$$

$$= 3.4\times10^{-4} L_{39.5} r_3^{-1}\left(\frac{h\nu_{\rm l}}{1\,{\rm MeV}}\right)^{-1}. \tag{20}$$

The luminosity and pair production would then be suppressed for very high-energy photons of $\gtrsim$ GeV.[4] Therefore, we expect that the pair-production rate will mostly be contributed by photons in keV–GeV bands.

Now, the density of positrons produced is

$$\frac{n_+}{n_{\rm e}} = \frac{\dot{n}_+ t_{\rm acc}}{n_{\rm e}} \tag{21}$$

$$= 8.4\times10^{-5} L_{39.5}^2 f_{3.5}^{-1} r_3^{-1.27}, \tag{22}$$

and hence the total positron production rate from the Sgr A* is

$$\dot{N}_+ = \dot{N}_{\rm w}\left(\frac{n_+}{n_{\rm e}}\right) \tag{23}$$

$$= 1.6\times10^{41} L_{39.5}^2 r_3^{-1}\ \ {\rm s}^{-1}. \tag{24}$$

Note that this estimate is per unit logarithmic interval of $\nu_{\rm h}$ (or $\nu_{\rm l}$). Since the Sgr A* luminosity during the increased activity can reliably be modeled up to $\sim$ MeV, the uncertainty is small for photons of $h\nu_{\rm l}\sim h\nu_{\rm h}\sim m_{\rm e}c^2$. Though it suffers larger uncertainty about the SED in the MeV–GeV bands, integration over $h\nu_{\rm h}\sim1\,{\rm MeV}$–$1\,{\rm GeV}$ would increase the total rate by a factor of 6.9. The rate has a large dependence on the accretion rate as $\dot{N}_+\propto L_\nu^2\propto f_{\rm b}^4$. Considering the model uncertainties, the two photon annihilation may also substantially contribute to the observed bulge 511 keV emission.

5.5. Comparison with Previous Studies

Positron production in RIAFs has been investigated in several previous studies (Kusunose, Mineshige 1996;

[3] The numerical factor $3\sqrt{\pi}$ of the nonrelativistic formula in Svensson [1982, equation (31)] should be corrected to $\pi\sqrt{3}$ as noted in Svensson (1984).

[4] Because of the increased luminosity compared with that of Sgr A* at present, this energy scale is much smaller than the estimate by Aharonian and Neronov (2005) for the present-day Sgr A* ($\sim$ 10 TeV).

Björnsson et al. 1996; EMN97); the results presented here are consistent with these in a sense that the effect of pair production in RIAFs is small, i.e., $n_+ \ll n_e$. However, the values of (n_+/n_e) found in this work are quantitatively higher than the results of EMN97 for stellar X-ray binaries, who found that the pair annihilation is in equilibrium with the pair production by electron-electron collisions, with a density ratio of $n_+/n_e \lesssim 10^{-5}$. The difference can be understood as follows.

As discussed in subsection 5.2, the criterion of the equilibrium between pair production and annihilation is given by $t_{acc}/t_{\pm,ann}$. According to the RIAF theory, we find the dependence of this quantity on the relevant parameters to be

$$\frac{t_{acc}}{t_{\pm,ann}} \propto \sigma_{\pm,ann}\frac{\dot{M}}{M_\bullet} \propto \sigma_{\pm,ann}\frac{\dot{M}}{\dot{M}_{Edd}}. \quad (25)$$

Though the Eddington accretion ratio, $\dot{M}/\dot{M}_{Edd}$, considered in this work is within the parameter range investigated by EMN97, $\sigma_{\pm,ann}$ is considerably different due to the difference in the electron temperature. In the two-temperature ADAF model considered by EMN97, the electron temperature is about the virial value, $T_e \sim 10^{9-10}$ K, while it is much higher in the RIAF model of Sgr A*, $T_e \sim 10^{11}$ K, because of the high value of δ (subsection 5.1). Since $\sigma_{\pm,ann} \propto \gamma_\pm^{-1} \sim \gamma_e^{-2}$, the value of $t_{acc}/t_{\pm,ann}$ for ADAF is much higher than in the model presented here, leading to pair equilibrium ($t_{acc} > t_{\pm,ann}$) as found by EMN97.

In pair equilibrium, the positron density is given by $n_+ \sim \dot{n}_+/(n_e\,\sigma_{\pm,ann}\,c)$. In the case of pair production by electron-electron collisions ($\dot{n}_+ \sim n_e^2\,\sigma_{ee}\,c$), we find that

$$\left(\frac{n_+}{n_e}\right)_{eq} \sim \frac{\sigma_{ee}}{\sigma_{\pm,ann}}. \quad (26)$$

In the model presented here, this value is $n_+/n_e \sim 0.15$ for $\gamma_e \sim 40$, and hence $n_+/n_e > 10^{-5}$ is possible, even if pair equilibrium is not reached. On the other hand, $\sigma_{\pm,ann}$ is much larger and σ_{ee} is smaller for the two-temperature ADAF having a lower T_e, leading to the low saturation value of $(n_+/n_e)_{eq} \lesssim 10^{-5}$ as found by EMN97.

Therefore, the higher electron temperature of the RIAF model of Sgr A* than the ADAF model, which is inferred from the fitting to observations, is essential for the present model to explain the 511 keV emission.

6. Positron Ejection from Sgr A*

6.1. Annihilation at the Production Site

Some of the positrons are lost by annihilation around the production site, producing direct annihilation gamma-ray emission from Sgr A*. Its spectrum depends on the positron spectrum and gravitational redshift, and it is thermal with a temperature of $T_e \sim 10$ MeV for electron-electron scattering. However, the small value of $(t_{acc}/t_{\pm,ann}) \sim \dot{n}_{\pm,ann}/\dot{n}_+ \sim 4.2\times10^{-2}\gamma_+^{-1}$ indicates that most of the produced positrons are conveyed into the SMBH or ejected by the wind. The direct annihilation gamma-ray luminosity from the pair-production site, $L_{\pm,ann} \sim (4\pi r_*^3/3)\dot{n}_{\pm,ann}$, is then much smaller than the positron production and ejection rate by the wind, $(n_+/n_e)\,\dot{N}_w \sim 4\pi\, s r_*^3 \dot{n}_+$.

6.2. Annihilation in the Wind

Here, we check that the positrons trapped in the outflow are not lost by annihilation before escaping the SMBH gravity. We assume a constant wind speed of $v_w \sim v_{esc}(r_*)$, and the density of the outflow is $n_w \sim \dot{N}_w/(4\pi r^2 v_w)$ for a steady wind. Then, the fraction of positrons that are lost by annihilation during wind propagation is

$$\eta_{ann} = \int_{r_*}^{\infty} n_w\,\sigma_{\pm,ann}\,v_\pm \frac{dr}{v_w}, \quad (27)$$

where $v_\pm$ is the relative velocity of electrons and positrons. Initially, both the electrons and positrons are relativistic, and hence $v_\pm \sim c$ and $\sigma_{\pm,ann} \propto \gamma_\pm^{-1} \sim (\gamma_e\gamma_+)^{-1} \propto r^{4/3}$, since γ_e and γ_+ scale as $\propto n_w^{1/3} \propto r^{-2/3}$ by adiabatic expansion. Either electrons or positrons become nonrelativistic at $r_{nr} = r_*\min(\gamma_{e*}, \gamma_{+*})^{3/2}$, and the scaling changes as $\sigma_{\pm,ann} \propto r^{2/3}$ at $r > r_{nr}$, where γ_{e*} and γ_{+*} are the Lorentz factor at the wind creation site ($r \sim r_*$). Then, $\sigma_{\pm,ann}v_\pm$ becomes constant after both electrons and positrons become nonrelativistic, since $\sigma_{\pm,ann} = \pi r_e^2/(v_\pm/c)$ in the nonrelativistic limit (Svensson 1982). Therefore, the main contribution to the integration comes from $r \sim r_{nr}$, and we obtain:

$$\eta_{ann} \sim 6\,n_w(r_{nr})\,\sigma_{\pm,ann}(r_{nr})\frac{c}{v_{esc}(r_*)}r_{nr} \quad (28)$$

$$\sim 6\,n_w(r_*)\,\sigma_{\pm,ann}(r_*)\frac{c}{v_{esc}(r_*)}r_*\left(\frac{r_{nr}}{r_*}\right)^{1/3} \quad (29)$$

$$= 1.5\times10^{-3} f_{3.5}\,\gamma_{+*}^{-1} r_3^{1.27}\,[\min(\gamma_{e*}, \gamma_{+*})]^{1/2}. \quad (30)$$

This is sufficiently small for any value of γ_{+*}, and hence we expect that almost all of the positrons produced around the SMBH will escape from the SMBH gravity field once they are trapped in the outflowing material.

6.3. On the Constraint from the Gamma-Ray Background Radiation

The above results indicate that the annihilation luminosity directly from Sgr A* is expected to be much smaller than the bulge 511 keV line emission in the phase of the past higher activity. The direct annihilation luminosity at present is even much smaller because of the current low accretion rate, far below the detection limit of gamma-ray telescopes in the foreseeable future.

This is important concerning the constraint from the diffuse gamma-ray background, whose flux is $E(dF/dE) \sim 10^{-4}$ photons cm^{-2} s^{-1} at ~ 1 MeV within 5° from the Galactic center (Beacom, Yüksel 2005). If any sources of the positrons directly emit annihilation gamma-rays before the injection of positrons into ISM, their spectrum would be broad around $\sim$ MeV, reflecting the positron spectrum and gravitational redshift. The flux from this process should not violate the observed MeV background, leading to an upper bound on the annihilation rate of $\lesssim 3.9\times10^{41}$ s^{-1}, assuming no positronium formation for annihilation within the source. Compared to the positron annihilation rate of $\sim 1.5\times10^{43}$ s^{-1} in ISM, the annihilation rate within the sources must be $\lesssim 2.6\%$ of the annihilation rate in ISM, if the sources are concentrated within 5° of the Galactic center. If the sources are distributed like

the observed 511 keV photons, the constraint becomes $\lesssim 10\%$, taking into account that $\sim 24\%$ of all the 511 keV photons come from the region within 5°.

The model presented here well satisfies this constraint, because of the current low accretion rate. However, it puts a stringent constraint on another explanation for the 511 keV emission by accreting black holes, i.e., LMXBs or microquasars. Theoretical models of pair production in these objects predict that most ($\sim 90\%$) of the produced pairs annihilate near the production site before injection into ISM (Guessoum et al. 2006), which is in serious conflict with the above constraint.

7. Positron Propagation in Interstellar Medium

7.1. Dynamics and Energetics of the Wind Injected into ISM

When positrons escape from the gravitational potential well of the SMBH, the kinetic energy of the outflow is expected to be dominant compared with the thermal energy because of adiabatic cooling, and hence the positron energy is determined by the bulk Lorentz factor, $\Gamma \sim 1$, of the wind, i.e., $\sim 1\,\mathrm{MeV}$, as argued in section 2. This is important, since too-relativistic outflow would be inconsistent with the observational upper bound on the injection energy, $\lesssim 3\,\mathrm{MeV}$ (Beacom, Yüksel 2005; Sizun et al. 2006). This bound is derived by a similar argument in the previous section (subsection 6.3), i.e., by requiring that gamma-rays from in-flight annihilation of positrons before thermalization in ISM do not make an excess of the diffuse gamma-ray background radiation.

The wind will sweep up ISM and heat it up by shocks. The ram pressure of the wind will be balanced with ISM at r_p, which is determined as $\dot{N}_\mathrm{w} m_\mathrm{p} v_\mathrm{w}/(4\pi r_\mathrm{p}^2) \sim P_\mathrm{ISM}$, assuming a quasi-isotropic wind. Assuming $P_\mathrm{ISM} = B^2/(8\pi)$ by an interstellar magnetic field of $B \sim 10\,\mu\mathrm{G}$ in the bulge region (LaRosa et al. 2005; Jean et al. 2006), we find $r_\mathrm{p} \sim 3.4 \times 10^2 f_{3.5}^{1/2} r_3^{-0.12} B_{10}^{-1}\,\mathrm{pc}$, where $B_{10} \equiv B/(10\,\mu\mathrm{G})$. This radius is comparable to the size of GCL or EMR, and also to the FWHM of the spatial extent of the 511 keV emission. Beyond $r \sim r_\mathrm{p}$, the shock-heated gas will expand by thermal pressure. Therefore, even if the wind originally has some anisotropy, it will not directly appear on a larger scale than $\sim r_\mathrm{p}$.

The observed expansion velocity of $\sim 100\,\mathrm{km\,s^{-1}}$ at the GCL/EMR region indicates an escape time of $t_\mathrm{esc} \sim 10^6\,\mathrm{yr}$ from this region. Thus, the wind kinetic energy stored in the GCL region is

$$E_\mathrm{GCL} \sim L_\mathrm{kin}\, t_\mathrm{esc} \tag{31}$$

$$\sim 1.5 \times 10^{55} f_{3.5}\, r_3^{-0.73} \left(\frac{t_\mathrm{esc}}{10^6\,\mathrm{yr}}\right)\ \mathrm{erg}. \tag{32}$$

This is interestingly similar to the energy of the hot gas ($kT \sim 8\,\mathrm{keV}$) in the Galactic center observed by X-rays (Koyama et al. 1989; Yamauchi et al. 1990; Muno et al. 2004), $E_\mathrm{hot} \sim 2.6 \times 10^{54} (r_\mathrm{p}/300\,\mathrm{pc})^{5/2}\,\mathrm{erg}$, where we obtained this value from the surface energy density estimated by Muno et al. (2004) assuming the size and depth to be $\sim r_\mathrm{p}$. In fact, the observed size of the hot gas ($\sim 1.^\circ 8$ FWHM: Koyama et al. 1989; Yamauchi et al. 1990) is in good agreement with r_p. Therefore, the large amount of energy stored in the hard X-ray emitting gas can be explained by the wind activity. The typical cooling time of the hot gas is $\sim 10^8\,\mathrm{yr}$ (Muno et al. 2004), which is much longer than t_esc, and hence the expansion is adiabatic, as argued by Sofue (2000) and Bland-Hawthorn and Cohen (2003). The expansion velocity ($\sim 100\,\mathrm{km\,s^{-1}}$) is much lower than the sound velocity of the hot gas ($\sim 10^3\,\mathrm{km\,s^{-1}}$), but it is possible if the associated cold material works as a ballast, as inferred from the infrared emission from expanding dust (subsection 3.2).

7.2. Positron Propagation Distance

At $r \gtrsim r_\mathrm{p}$, positrons are expected to interact with ISM and produce 511 keV emission. In the hot phase of ISM, which is the dominant component in the volume-filling factor in the bulge region (Jean et al. 2006), positrons are thermalized on a time scale of $\sim 3 \times 10^6\,\mathrm{yr}$, and then annihilate on a time scale of $\sim 10^7\,\mathrm{yr}$ (Guessoum et al. 2005; Jean et al. 2006). Therefore, the time scale of the past higher activity inferred from the outflow evidence is sufficient to explain the 511 keV line emission. Positrons can maximally reach $\sim 1\,\mathrm{kpc}$ by large-scale outflow ($\sim 100\,\mathrm{km\,s^{-1}}$) within this time scale, being consistent with the observed maximum extent of the 511 keV emission ($\sim 20^\circ$). Most positrons must annihilate before traveling this distance, since the spectral analysis of the 511 keV line indicates that almost all positrons are annihilating in a warm neutral or warm ionized phase of ISM (Jean et al. 2006), where the annihilation time scale is much shorter. An exact spatial profile of the 511 keV line emission would be determined by the probability of positrons entering into the warm phase of ISM at $r \gtrsim r_\mathrm{p}$.

Diffusion in a random magnetic field should also have a significant effect. Jean et al. (2006) estimated the propagation length by quasilinear diffusion for MeV positrons in the bulge as $\sim 260\,\mathrm{pc}$ for a time scale of $\sim 3 \times 10^6\,\mathrm{yr}$, using a diffusion coefficient of $D \sim 9.8 \times 10^{-4}\,\mathrm{kpc^2\,Myr^{-1}}$, which was derived from $B = 10\,\mu\mathrm{G}$ and the Kolmogorov turbulent spectrum. Though the Kolmogorov spectrum is not valid for cosmic-ray propagation in the Galactic disk (Maurin et al. 2001), this is not significant because a similar diffusion coefficient of $4.1 \times 10^{-4}\,\mathrm{kpc^2\,Myr^{-1}}$ is obtained using the parameters derived by Maurin et al. (2001) to explain the cosmic-ray data around the solar system.

A more detailed, quantitative prediction about the 511 keV line morphology is beyond the scope of this paper, but these considerations indicate that the model presented here is broadly consistent with the observed morphology and spatial extent of the 511 keV line emission.

8. Discussion

8.1. Comparison with Other Models of the Positron Production from Sgr A*

Titarchuk and Chardonnet (2006) proposed a scenario in which positrons are produced by the annihilation of hard X-ray and $\sim 10\,\mathrm{MeV}$ photons around Sgr A*. The hard X-ray photons are emitted from the accretion activity of the SMBH, while the $\sim 10\,\mathrm{MeV}$ photons are produced by accretion onto hypothetical small mass black holes (SmMBHs) with a mass of $\sim 10^{17}\,\mathrm{g}$ ($\sim 10^{-16}\,M_\odot$), which are assumed to be distributed within $r \sim 10^{2-3}\,r_\mathrm{s}$ of the SMBH. If they are accreting with the

Eddington accretion rate, and their density is comparable to the dark matter, the SmMBHs can supply enough 10 MeV photons for the required pair production. Such SmMBHs have not yet been excluded as a candidate of the dark matter, but there is no strong theoretical motivation, in contrast to the well-motivated dark-matter candidates, such as neutralinos (e.g., Bertone et al. 2004). Furthermore, it is extremely difficult to supply the accreting material onto such SmMBHs at the Eddington rate by Bondi accretion; the Bondi accretion rate for a 10^{17} g SmMBH with typical parameters is

$$\dot{M}_{\rm B} \sim 7.9 \times 10^{-23} \left(\frac{n_{\rm e}}{\rm cm^{-3}}\right) \left(\frac{kT}{1\,\rm eV}\right)^{-3/2} \ {\rm g\,s^{-1}}, \qquad (33)$$

which should be compared with the Eddington accretion rate of $\dot{M}_{\rm Edd} = 72\,{\rm g\,s^{-1}}$. The difference is almost 24 orders of magnitude, and it seems quite unlikely that such SmMBHs have the Eddington accretion rate under any realistic astrophysical circumstances.

Cheng, Chernyshov, and Dogiel (2006) considered cosmic-ray production by a jet or outflow from the SMBH, which is ejected when stars are captured by the SMBH. In their scenario, the cosmic rays produce pions by collisions with ISM, and then positrons are produced by pion decays. The most important difference between this model and that proposed in this paper is the high injection energy into ISM ($\gtrsim 30$ MeV) of pion-decay positrons. Such a high injection energy is inconsistent with the observational upper bound on the injection energy, $\lesssim 3$ MeV, as mentioned in subsection 7.1.

Another problem about positron production from pion decays is the observed large bulge-to-disk ratio of the 511 keV line emission. We know that the Galactic gamma-ray background in the GeV band is mainly composed of pion-decay gamma-rays produced by cosmic-ray interactions in ISM (Strong et al. 2000, 2004), i.e., the same process with the model of Cheng, Chernyshov, and Dogiel (2006). The GeV background is clearly associated along with the Galactic disk, and we have a difficulty in explaining why we do not see the strong disk component of the 511 keV emission if it is produced by the cosmic-ray interactions.

8.2. Predictions and Possible Tests by Future Observations

Although a quantitative prediction of the morphology of the 511 keV emission is beyond the scope of this paper, it could be more spherically asymmetric in comparison with other explanations, such as SNe Ia or MeV-mass dark matter. Asymmetry is expected by the wind anisotropy in the region of $r \lesssim r_{\rm p} \sim$ a few degrees, or by matter distribution in the Galaxy at $r \gtrsim r_{\rm p}$. Asymmetry has not yet been detected in the observed 511 keV morphology (Knödlseder et al. 2005), but it does not reject the model presented here because of the limited angular resolution of the SPI spectrometer of INTEGRAL ($\sim 3^\circ$ FWHM) and the large uncertainty of the theoretical expectation for the anisotropy. Future observational studies on the 511 keV morphology with better angular resolution might, however, detect larger asymmetry than that expected from the other explanations.

Another prediction of the proposed scenario is that it is extremely difficult to detect 511 keV emission in regions other than the Galactic bulge from the source population that is responsible for the bulge component. SMBHs are generally found in galaxies having bulges, and the nearest SMBH is probably M 31* in the Andromeda galaxy. The X-ray luminosity of M 31* is $\sim 10^{36}\,{\rm erg\,s^{-1}}$ (Garcia et al. 2005), which is about 10^3 times larger than the quiescent phase of Sgr A*, but 10^3 times smaller than the past higher activity phase. If this X-ray luminosity reflects the typical activity averaged over a time scale of $\sim 10^7$ yr, we expect that the 511 keV luminosity of the M31 bulge is much fainter than that of the Galaxy. The 511 keV emission has been detected at $\sim 50\sigma$ level (Knödlseder et al. 2005), and considering that the distance to M 31 is 770 kpc, a large improvement of the sensitivity is required.

On the other hand, there is a good chance of detecting 511 keV emission anywhere other than the Galactic bulge, for some other models of the bulge 511 keV emission (e.g., Knödlseder et al. 2005). For example, if the origin is SNe Ia, improved instruments in the near future will detect 511 keV line emission from nearby supernova remnants. In fact, an interesting limit on the positron escape fraction from SN 1006 has already been obtained (Kalemci et al. 2006). If the origin is MeV-mass dark matter annihilation, we expect to observe the 511 keV line emission from nearby dwarf galaxies by a modest improvement of the sensitivity. If future negative results rule out other explanations of the 511 keV emission, it would strengthen the case for the scenario presented here.

It should also be noted that the standard prediction for positron production from SNe Ia is only one order of magnitude short of that required to explain the bulge 511 keV emission (Prantzos 2006). Therefore, just a detection of 511 keV emission from a nearby SN Ia does not confirm SNe Ia as the origin of the bulge component, but a close examination of the positron production efficiency would be required.

9. Conclusion

In this paper, it has been shown that the several independent lines of evidence for the past higher activity of the Galactic center (i.e., higher X-ray luminosity and large scale outflows) can be quantitatively explained by the RIAF model of Sgr A*, in which energetic outflow plays an essential role. A single increased accretion rate from the current value explains both the past high X-ray luminosity and the kinetic luminosity of the outflow inferred from observations. The required boost factor of the accretion rate is about 10^{3-4} for a time scale of $\sim 10^7$ yr in the past. We have shown that this accretion rate and its duration are naturally expected in the environment of the Galactic center. The outflow is energetic enough to supply heat to maintain the hot (~ 8 keV) plasma observed in the Galactic center region, for which there have been no clear explanation. The current low accretion rate is likely to be caused by a sudden destruction of the accretion flow when the shell of the supernova remnant Sgr A East passed through the SMBH about 300 yr ago. The chance probability of observing Sgr A* in such a low-activity phase is estimated to be $\sim 0.5\%$.

We then estimated the production rate of positrons during the high-activity phase, which are created in the region around the event horizon, and then ejected by the outflow. The

rate is found to be comparable with that required to explain the 511 keV line emission toward the Galactic bulge. We considered three processes of $e^{\pm}$ pair-production: electron-electron scattering, photon-electron collision, and photon-photon annihilation. Interestingly, all three processes give a similar positron production rate.

Therefore, the model presented here gives a new and natural explanation for the 511 keV line emission toward the Galactic bulge. The favorable aspects of this model are: (1) the correct positron production rate, (2) the large bulge-to-disk ratio and correct spatial extent in the bulge, (3) (i) negligible annihilation near the positron production site before injection into ISM, and (ii) the injection energy of $\sim$ MeV, both of which are important to meet the constraint from the MeV gamma-ray background, and (4) no exotic assumptions or parameters. To our knowledge, the other explanations for the 511 keV emission proposed so far do not satisfy all of these.

Anisotropy of the morphology of the 511 keV emission larger than that expected for other models would be a signature for the model proposed here, which might be revealed by future observations with better angular resolutions. The detection of 511 keV lines from the centers of nearby galaxies by the same mechanism will be difficult even in the foreseeable future. In contrast, some other scenarios predict detectable 511 keV lines in directions other than the Galactic center by a modest improvement of the sensitivity.

We would like to thank an anonymous referee for useful comments. This work was supported by a Grant-in-Aid for the 21st Century COE "Center for Diversity and Universality in Physics" from the Ministry of Education, Culture, Sports, Science and Technology (MEXT).

References

Aharonian, F., et al. 2004, A&A, 425, L13
Aharonian, F., & Neronov, A. 2005, ApJ, 619, 306
Anantharamaiah, K. R., Pedlar, A., & Goss, W. M. 1999, ASP Conf. Ser., 186, 422
Baganoff, F. K., et al. 2003, ApJ, 591, 891
Beacom, J. F., & Yüksel, H. 2005, Phys. Rev. Lett., 97, 071102
Bertone, G., Hooper, D., & Silk, J. 2004, Phys. Rep., 405, 279
Björnsson, G., Abramowicz, M. A., Chen, X., & Lasota, J.-P. 1996, ApJ, 467, 99
Blandford, R. D., & Begelman, M. C. 1999, MNRAS, 303, L1
Bland-Hawthorn, J., & Cohen, M. 2003, ApJ, 582, 246
Cheng, K. S., Chernyshov, D. O., & Dogiel, V. A. 2006, ApJ, 645, 1138
Cuadra, J., Nayakshin, S., Springel, V., & di Matteo, T. 2006, MNRAS, 366, 358
Diehl, R., et al. 2006, Nature, 439, 45
Eisenhauer, F., Schödel, R., Genzel, R., Ott, T., Tecza, M., Abuter, R., Eckart, A., & Alexander, T. 2003, ApJ, 597, L121
Esin, A. A., McClintock, J. E., & Narayan, R. 1997, ApJ, 489, 865 (EMN97)
Falcke, H., & Biermann, P. L. 1999, A&A, 342, 49
Gallo, E., Fender, R., Kaiser, C., Russell, D., Morganti, R., Oosterloo, T., & Heinz, S. 2005, Nature, 436, 819
Gallo, E., Fender, R. P., & Pooley, G. G. 2003, MNRAS, 344, 60
Garcia, M. R., Williams, B. F., Yuan, F., Kong, A. K. H., Primini, F. A., Barmby, P., Kaaret, P., & Murray, S. S. 2005, ApJ, 632, 1042
Genzel, R., Eckart, A., Ott, T., & Eisenhauer, F. 1997, MNRAS, 291, 219
Guessoum, N., Jean, P., & Gillard, W. 2005, A&A, 436, 171
Guessoum, N., Jean, P., & Prantzos, N. 2006, A&A, 457, 753
Ho, L. C. W. 2004, in Coevolution of Black Holes and Galaxies, ed. L. C. Ho (Cambridge: Cambridge University Press), 292
Hooper, D., & Dingus, B. L. 2004, Phys. Rev. D, 70, 113007
Jean, P., Knödlseder, J., Gillard, W., Guessoum, N., Ferrière, K., Marcowith, A., Lonjou, V., & Roques, J. P. 2006, A&A, 445, 579
Kaifu, N., Kato, T., & Iguchi, T. 1972, Nature, 238, 105
Kalemci, E., Boggs, S. E., Milne, P. A., & Reynolds, S. P. 2006, ApJ, 640, L55
Kato, S., Fukue, J., & Mineshige, S. 1998, Black-Hole Accretion Disks (Kyoto: Kyoto University Press)
Knödlseder, J., et al. 1999, A&A, 344, 68
Knödlseder, J., et al. 2005, A&A, 441, 513
Koyama, K., et al. 2006, PASJ, 59, S245
Koyama, K., Awaki, H., Kunieda, H., Takano, S., & Tawara, Y. 1989, Nature, 339, 603
Koyama, K., Maeda, Y., Sonobe, T., Takeshima, T., Tanaka, Y., & Yamauchi, S. 1996, PASJ, 48, 249
Kusunose, M., & Mineshige, S. 1996, ApJ, 468, 330
LaRosa, T. N., Brogan, C. L., Shore, S. N., Lazio, T. J., Kassim, N. E., & Nord, M. E. 2005, ApJ, 626, L23
Le, T., & Becker, P. A. 2004, ApJ, 617, L25
Maeda, Y., et al. 2002, ApJ, 570, 671
Martini, P. 2004, in Coevolution of Black Holes and Galaxies, ed. L. C. Ho (Cambridge: Cambridge University Press), 169
Maurin, D., Donato, F., Taillet, R., & Salati, P. 2001, ApJ, 555, 585
Mayer-Hasselwander, H. A., et al. 1998, A&A, 335, 161
Mineshige, S., Kusnose, M., & Matsumoto, R. 1995, ApJ, 445, L43
Muno, M. P., et al. 2004, ApJ, 613, 326
Murakami, H., Koyama, K., & Maeda, Y. 2001a, ApJ, 558, 687
Murakami, H., Koyama, K., Sakano, M., Tsujimoto, M., & Maeda, Y. 2000, ApJ, 534, 283
Murakami, H., Koyama, K., Tsujimoto, M., Maeda, Y., & Sakano, M. 2001b, ApJ, 550, 297
Narayan, R., Mahadevan, R., & Quataert, E. 1998, in Theory of Black Hole Accretion Disks, ed. M. A. Abramowicz, G. Björnsson, & J. E. Pringle (Cambridge: Cambridge University Press), 148
Narayan, R., & McClintock, J. E. 2005, ApJ, 623, 1017
Narayan, R., & Quataert, E. 2005, Science, 307, 77
Ohsuga, K., Kato, Y., & Mineshige, S. 2005, ApJ, 627, 782
Paumard, T., et al. 2006, ApJ, 643, 1011
Pedlar, A., Anantharamaiah, K. R., Ekers, R. D., Goss, W. M., van Gorkom, J. H., Schwarz, U. J., & Zhao, J.-H. 1989, ApJ, 342, 769
Prantzos, N. 2006, A&A, 449, 869
Prantzos, N., & Diehl, R. 1996, Phys. Rep., 267, 1
Revnivtsev, M. G., et al. 2004, A&A, 425, L49
Revnivtsev, M., Sazonov, S., Gilfanov, M., Churazov, E., & Sunyaev, R. 2006, A&A, 452, 169
Salamon, M. H., & Stecker, F. W. 1998, ApJ, 493, 547
Schödel, R., Ott, T., Genzel, R., Eckart, A., Mouawad, N., & Alexander, T. 2003, ApJ, 596, 1015
Scoville, N. Z. 1972, ApJ, 175, L127
Sizun, P., Cassé, M., & Schanne, S. 2006, Phys. Rev. D., 74, 063514
Sofue, Y. 2000, ApJ, 540, 224
Strong, A. W., Moskalenko, I. V., & Reimer, O. 2000, ApJ, 537, 763
Strong, A. W., Moskalenko, I. V., & Reimer, O. 2004, ApJ, 613, 962

Svensson, R. 1982, ApJ, 258, 335
Svensson, R. 1984, MNRAS, 209, 175
Titarchuk, L., & Chardonnet, P. 2006, ApJ, 641, 293
Yamauchi, S., Kawada, M., Koyama, K., Kunieda, H., & Tawara, Y. 1990, ApJ, 365, 532
Yuan, F., Markoff, S., & Falcke, H. 2002, A&A, 383, 854
Yuan, F., Quataert, E., & Narayan, R. 2003, ApJ, 598, 301 (YQN03)
Yuan, F., Quataert, E., & Narayan, R. 2004, ApJ, 606, 894 (YQN04)
Yusef-Zadeh, F., Melia, F., & Wardle, M. 2000, Science, 287, 85
Zdziarski, A. A. 1982, A&A, 110, L7
Zdziarski, A. A. 1985, ApJ, 289, 514